THE HUMAN INSULA: ARCHITECTONIC ORGANIZATION AND POSTMORTEM MRI REGISTRATION

A. MOREL, [a]* M. N. GALLAY, [a†] A. BAECHLER, [a]
M. WYSS [b] AND D. S. GALLAY [a††]

[a] *Center for Clinical Research, University Hospital Zürich, Sternwartstrasse 6, CH-8091 Zürich, Switzerland*

[b] *Institute for Biomedical Engineering, University Hospital Zürich, Zürich, Switzerland*

Abstract—The human insula has been the focus of great attention in the last decade due to substantial progress in neuroimaging methodology and applications. Anatomical support for functional localization and interpretations, however, is still fragmented. The aim of the present study was to re-examine the microanatomical organization of the insula and relate cytoarchitectonic maps to major sulcal/gyral patterns by registration to high-resolution MR images of the same brains. The insula was divided into seven architectonic subdivisions (G, Ig, Id1–3, Ia1–2) that were charted on unfolded maps of the insula following a method used previously in monkeys. The results reveal overall similar patterns of Nissl, and to some extent also, myelin and parvalbumin (PV), as in monkeys, with a postero-dorsal to antero-ventral gradient of hypergranular to granular, dysgranular and agranular fields. Reversals occur ventrally along the inferior peri-insular sulcus (IPS), at the margin with the temporal operculum, and anteriorly at the limit with orbitofrontal cortex (OFC). A large portion of agranular cortex is characterized by a dense accumulation of the spindle-shaped von Economo neurons (VENs) in layer V. The distribution of VENs is not restricted to agranular insula but also extends into the anterior part of dysgranular fields. The patterns of intracortical myelin and of PV neuropil in the middle layers follow decreasing gradients from postero-dorsal granular to antero-ventral agranular insula, with particularly strong staining in posterior and dorsal insula. A separate PV enhanced area in the middle-dorsal insula corresponds in location to the presumed human gustatory area. Projections of the cytoarchitectonic maps onto high-resolution stereotactic MRI reveal a near concentric organization around the limen insula, with each cytoarchitectonic subdivision encompassing several major insular gyri/sulci. The dysgranular domain is the largest, taking up about half of the insula. The present study of the human insula provides a new anatomical basis for MR imaging and clinical applications.

© 2013 IBRO. Published by Elsevier Ltd.

Key words: Island of Reil, cytoarchitecture, myelin, parvalbumin, MRI projections, Von Economo neurons.

*Corresponding author. Tel: +41-44-255-4036; fax: +41-44-255-5741.
E-mail addresses: aemorel@gmail.com, anne.morel@usz.ch (A. Morel).
† Current address: Kantonsspital St. Gallen, Klinik für Neurochirurgie, Rorschacherstrasse 95, CH-9007 St. Gallen, Switzerland.
†† Current address: Spital Rorschach, Kantonsspital St.Gallen, Klinik für Chirurgie, Heidenerstrasse 11, CH-9400 Rorschach, Switzerland.

Abbreviations: Ac, anterior commissure; ag, accessory insular gyrus; alg, anterior long insular gyrus; APS, anterior peri-insular sulcus; asg, anterior short insular gyrus; BB, band of Baillarger; CIS, central insular sulcus; FI, frontoinsular; G, hypergranular field; HG, Heschl's gyrus; Ia, agranular insula; Id, dysgranular insula; Ig, granular insula; IPS, inferior peri-insular sulcus; Li, limen insula; msg, middle short insular gyrus; OFC, orbitofrontal cortex; pc, posterior commissure; PCIS, precentral insular sulcus; PIS, postcentral insular sulcus; plg, posterior long insular gyrus; Poc, piriform olfactory cortex; psg, posterior short insular gyrus; PuT, putamen; PV, parvalbumin; RI, retroinsular cortex; SIS, short insular sulcus; SPS, superior peri-insular sulcus; STP, superior temporal plane; tg, transverse insular gyrus; VENs, Von Economo neurons.

INTRODUCTION

The human insula has attracted major interest in the last decade due to considerable progress in neuroimaging and to data collected during intraoperative functional explorations. These studies confirm earlier observations of the involvement of the "fifth lobe" of the brain in a variety of functions, from sensory to motor, cognitive, affective and visceral (Augustine, 1985; Mesulam and Mufson, 1985; Craig et al., 2000; Peyron et al., 2000; Frot and Mauguiere, 2003; Brooks et al., 2005; Mutschler et al., 2009; Ackermann and Riecker, 2010; Small, 2010; Kurth et al., 2010a; Cauda et al., 2011; Pugnaghi et al., 2011; Stephani et al., 2011; Nieuwenhuys, 2012a). Localization in the insula is often related to a bipartite antero-posterior division separated by the central insular sulcus, with different functions attributed to the posterior versus anterior insula. For example, processing of pain has been particularly emphasized in the posterior insula and adjoining opercular areas (Ostrowsky et al., 2002; Frot et al., 2007; Garcia-Larrea et al., 2010; Mazzola et al., 2012b) while the anterior insula is more implicated in the integration of complex autonomic, cognitive and emotional process thought to be important in interoceptive awareness (Craig, 2009; Allman et al., 2010; Zaki et al., 2012). More recently, the possibility to explore *in vivo* human brain connectivity (using probabilistic diffusion tractography and resting-state functional connectivity) provided interesting insight into insular organization and relation to architectonic parcellation (Cauda et al., 2011; Cerliani et al., 2012; Cloutman et al., 2012; Jakab et al., 2012), though current resolution still prevents close correlations.

In contrast to the plethora of neuroimaging studies, relatively little progress has been made in the detailed

analysis of the architectonic organization of the human insula in relation to its major gyri and sulci. Comparing with the monkey's insula, Mesulam and Mufson (1985) proposed a similar cytoarchitectonic organization in humans with three major domains, agranular, dysgranular and granular concentrically arranged around the Piriform olfactory cortex (Poc) at the limen insula (Li). However, the relatively sparse description and pictorial representation cannot easily be related to the complex anatomy of the human insula presented in postmortem and *in vivo* neuroimaging studies. More recently, two studies provided more insight into cytoarchitectonic organization of the human insula. In the first, a map was produced to evaluate insular pathological changes in Alzheimer disease (Bonthius et al., 2005) and showed corresponding overall gradients described by Mesulam and Mufson (1985) and by a tentative representation in a Golgi study of the insula (Anderson et al., 2009). In the second, Kurth et al. (2010b) using an "observer-independent" approach, present a probabilistic map of the posterior insula which differs somewhat from the other schemes, in particular with regard to the extension of the granular domain. Other studies devoted to the orbital and medial prefrontal cortex (Ongur et al., 2003) and including most anterior part of the insula defined several subdivisions on the basis of cyto- and chemoarchitectonic criteria. This same region, also called the frontoinsular cortex (FI), stands out, particularly in human and great apes, by the presence in layer V of large spindle-shaped, bipolar neurons (so-called VENs) similar to those also found in anterior cingulate cortex (Von Economo and Koshinas, 1925; Nimchinsky et al., 1995; Von Economo, 2009; Allman et al., 2010; Butti and Hof, 2010). These VENs are thought to play a role in intuition and be specifically affected in several neuropsychiatric disorders with deficits in emotional functions (Allman et al., 2005; Seeley, 2010; Butti et al., 2013; Santos et al., 2011; Kim et al., 2012).

Given the current fragmented knowledge of the microanatomical organization of the human insula, the present study was undertaken to 1) provide detailed cytoarchitectonic maps of the human insula using a similar approach as in monkeys (Gallay et al., 2012), and 2) correlate cytoarchitectonic organization with insular surface landmarks by 2D registration to high-resolution stereotactic MRI of the same brains. A similar approach has already been used to improve the localization of human cortical areas (Walters et al., 2003; Eickhoff et al., 2006a; Blaizot et al., 2010; Uylings et al., 2010) for functional imaging and clinical applications. Preliminary results were presented in abstract form (Gallay et al., OHBM, 2011).

EXPERIMENTAL PROCEDURES

This work is based on the analysis of four specimens obtained from postmortem brains provided by the Department of Pathology (Hospital Münsterlingen, Switzerland) and the Departments of Anatomy (Universities of Basel and Bern, Switzerland). Information on age, gender and postmortem delay was available for two brains: Hb1 (57 years, female, 24 h) and Hb2 (68 years, male, < 48 h) that were fixed in formalin 10% for 6 weeks (Hb1) and 3 months (Hb2) before histological processing. Both brains were from normal subjects with no neuropathological signs at autopsy. For cases Hb3 and Hb4, the brains were obtained about 2 years after autopsy had been performed and had been fixed in formalin. All procedures were conducted in accordance with the Declaration of Helsinki.

MR image acquisition

MR imaging was performed on 3.0T and 7.0T Philips Achieva systems (Philips Healthcare, Best, The Netherlands, and Cleveland, Ohio, USA, respectively) and for one specimen on a 3.0T Siemens Verio system (Siemens Healthcare, Erlangen, Germany) (see Table 1). The brain specimens were placed in a plastic container filled with phosphate buffer 0.1 M (PB) or formalin, and fixed with pieces of plasticine to prevent motion during scanning. MR protocols included several sequences and those used for MRI registrations are given in details in Table 1. For whole brain scanning an eight channel Head coil, in one case (Hb4) an eight channel Knee coil, were used. For blocks of the insula that were obtained by guillotine section (Morel, 2007) a two channel surface coil was used. On the 7.0T Scanner a quadrature transmit and receive surface coil (RAPID Biomedical GmbH, Rimpar, Germany) was used. In order to get the best possible SNR (signal to noise ratio), in each case the smallest possible coil was chosen according to the size of the specimen. In the Multiecho 2D Turbo Spin Echo sequences, all five echoes were combined together to improve SNR and CNR (contrast to noise ratio).

Tissue preparation and histology

After MR scanning, the insula blocks, in whole or divided into 2 or 3 smaller blocks, were cryoprotected in successive concentrations of sucrose (10%, 20% and 30%) in PB, then frozen at ~−30 °C in isopentan and stored at −75 °C. Cryostat sections were cut at 50 μm in coronal (cases Hb1-L, Hb2-L, Hb3-R) or horizontal (case Hb4-L) planes and several series were collected in PB and immediately mounted on gelatinized slides or stored in PB or formalin 10% for later processing. Histological procedures were similar to those described previously for the human thalamus (Morel, 2007; Gallay et al., 2008) with few modifications. Adjacent series of sections (500 μm apart) were stained for Nissl, with Cresyl-Violet, myelin, with the Black-Gold II complex (Histo-Chem Inc, Jefferson, USA) or immunostained with a mouse monoclonal antibody against the calcium-binding protein parvalbumin (PV) (Swant swiss antibodies, Marly, Switzerland). For PV immunostaining, the best results were obtained with primary antibody concentrations of 1:1000 and 1:2000. For details of the immunocytochemical procedure, we refer to (Gallay et al., 2008). For myelin staining, the Black-Gold II complex procedure (Walters et al., 2003; Schmued et al., 2008) was applied to mounted sections: after several rinses in acetic acid 1%, sections were incubated at 60 °C in 0.3% Black-Gold solution for 20–40 min. Sections were then rinsed in distilled water, fixed in 3% sodium thiosulfate, dehydrated in alcohols and coverslipped.

Data analysis

Contours of the insula and adjoining opercular cortex, positions of sulci/gyri and of architectonic borders were plotted at regular intervals (500–1000 μm) using a Leica (DM 6000 B) microscope equipped with a digital camera (MBF CX 9000) and a computerized plotting system (Neurolucida, Micro-BrightField,

Table 1. Postmortem MRI protocols

Specimen	Anatomy	Protocol	Scanner	Coil
Hb2	Whole brain	T1w MPRAGE FOV: 268 × 268 mm², 256 slices Matrix: 384 × 384 Resolution: 0.7 × 0.7 × 0.7 mm³ TR:2000 ms, TE: 2.7 ms Time inversion: 700 ms, flipangle: 8° 12 signal averages, scantime: 2:34 h	3.0T Verio	8ch Head Coil
Hb3	Whole brain	Multiecho 2D Turbo Spin Echo FOV: 160 × 160 mm², 52 slices Matrix: 1068 × 1068 Resolution: 0.15 × 0.15 × 1.2 mm³ TR: 3900 ms, TE: 13 ms, 25 ms, 38 ms, 51 ms, 64 ms, ETL: 5, bandwidth:195 Hz/pixel 5 signal averages, scantime: 11 h	3.0T Achieva	8ch Head Coil
Hb3	R-insula bloc	Multiecho 2D Turbo Spin Echo FOV: 160 × 160 mm², 52 slices Matrix: 576 × 576 Resolution: 0.15 × 0.15 × 0.9 mm³ TR: 5300 ms, TE: 13 ms, 25 ms, 38 ms, 51 ms, 64 ms, ETL: 5, bandwidth: 195 Hz/pixel 5 signal averages, scantime: 11 h	3.0T Achieva	2ch Surface Coil
Hb4	L-hemisphere	Multiecho 2D Turbo Spin Echo FOV: 120 × 120 mm²,60 slices Matrix: 600 × 600 Resolution: 0.2 × 0.2 × 1.2 mm³ TR: 3400 ms, TE: 11 ms, 22 ms, 33 ms, 43 ms, 54 ms, ETL: 5, bandwidth: 214 Hz/pixel 5 signal averages, scantime: 5 h 44 min	3.0T Achieva	8ch Knee Coil
Hb4	L-insula bloc	3D PDW Turbo Spin Echo FOV: 110 × 100 mm², 350 slices Matrix: 768 × 732 Resolution: 0.15 × 0.15 × 0.2 mm³ TR: 900 ms, TE: 14 ms ETL: 14, bandwidth: 242 Hz/pixel 1 signal average, scantime: 4 h 33 min	7.0T Achieva	Extremity T/R

Inc., Williston, VT, USA). The Neurolucida plots were exported as vector data to Adobe Illustrator and superposed onto scans of stained sections.

Unfolded maps. In order to compare the overall cytoarchitectonic organization of the insula between cases, unfolded maps were produced using a similar approach as in monkeys (Gallay et al., 2012). For unfolded maps reconstructed from coronal sections, distances measured along layer IV, or between layer III and V, were plotted from the superior peri-insular sulcus (SPS) to the inferior peri-insular sulcus (IPS) in the posterior insula, to the lateral limb (IPS-l) or a short distance beyond the sulcus in the middle insula, and to the fronto-orbital limb of the annectant gyrus (ag) in anterior insula. The procedure is illustrated in Fig. 1 where the positions of cytoarchitectonic borders delimited on a coronal section at mid-insular level are plotted on a vertical line orthogonal to the axis of the SPS (reference horizontal line, right panel). For the unfolded map reconstructed from horizontal sections (case Hb4-L, Fig. 9), the reference is represented by the IPS and is indicated by a vertical line on the right-hand part of the map that was re-oriented to better compare with the other cases.

MRI registration. Cytoarchitectonic borders and positions of sulci were first projected onto corresponding coronal or horizontal MRI (at 1–2 mm intervals) using gyral/sulcal morphology of the insula and adjacent opercular cortex to align the sections. For comparison between cases, cytoarchitectonic subdivisions were then plotted on sagittal MRI obtained from 3D reconstructions using eFilm v.3.0 software (Merge

Healthcare, Wisconsin, USA). The method is illustrated in Fig. 6 for the case of Hb3-R. On each coronal MRI, the position of sagittal planes selected for the final maps are represented by vertical lines. The extent of cytoarchitectonic fields encountered in grey matter (determined by changes in MR contrast and aided by superposition of Nissl sections) are displayed by colored segments, with color codes corresponding to subdivisions represented in unfolded maps. The position of stereotactic planes (centers of the anterior commissure (ac), posterior commissure (pc), and the intercommissural plane, DV0) is represented on each sagittal map. A more global representation of the cytoarchitectonic organization in the sagittal plane was obtained by projecting cytoarchitectonic segments on the surface of the insula (see upper panels Fig. 7). A similar procedure was applied for projections on sagittal MRI of cytoarchitectonic subdivisions delineated on horizontal sections (Fig. 9). In this case, sections did not include the ventral tiers of the insula.

Terminology

Insular cytoarchitectonic parcellation follows the classical division into granular, dysgranular and agranular domains in a dorso-posterior to ventral direction, with additional subdivisions comparable to those defined previously in monkeys (Gallay et al., 2012). For topographical landmarks, the nomenclature of major insular gyri and sulci is based on the anatomical study by Ture et al. (1999). Their identification was facilitated on sagittal views of the insula in post-mortem MRI.
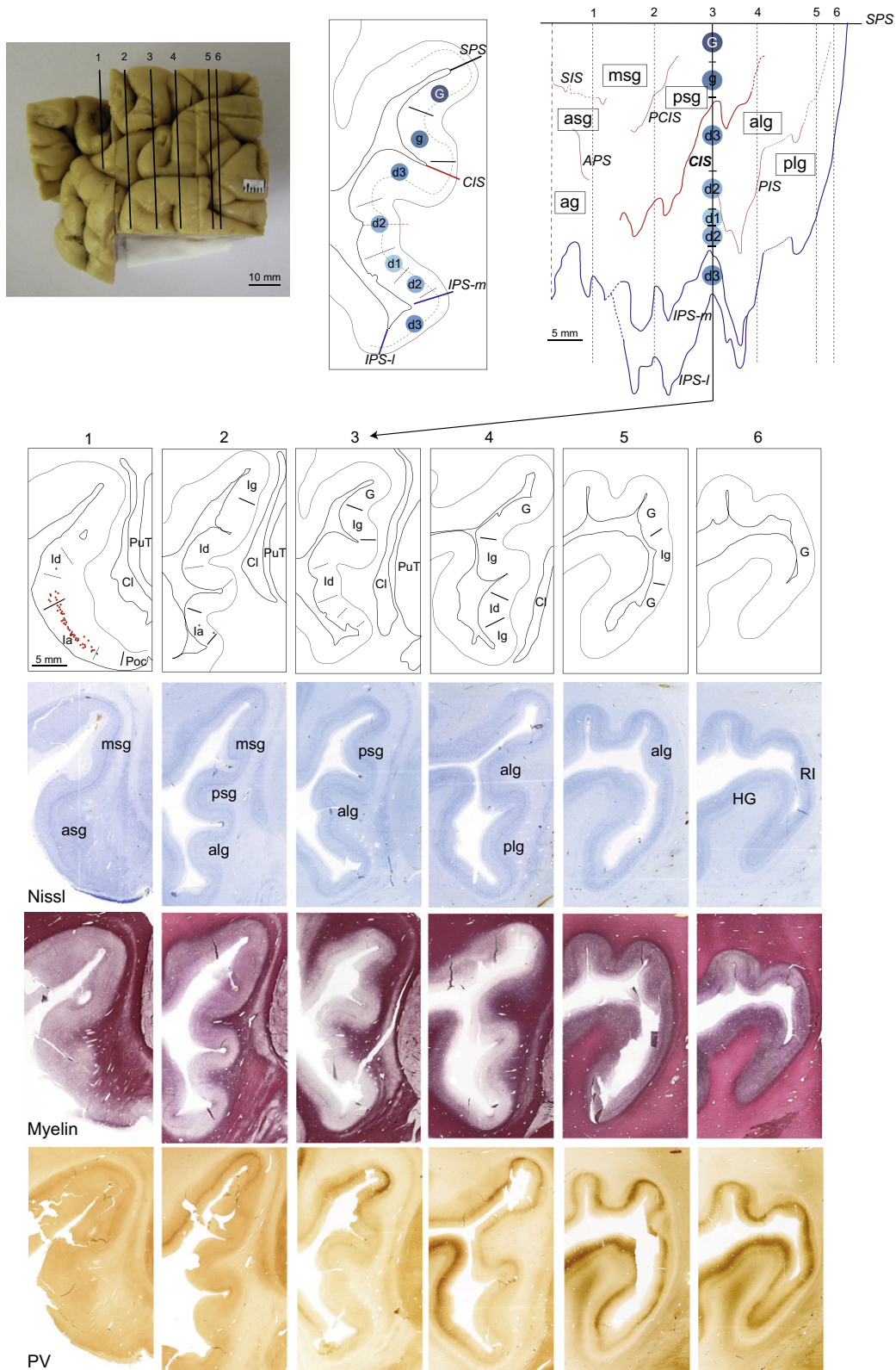
Fig. 1. Multiarchitectonic characteristics of the human insula. Lower panels represent Nissl, myelin and PV-stained coronal sections (case Hb2-L) and corresponding drawings of the cytoarchitectonic boundaries and subdivisions. Dotted lines indicate borders between subsectors of granular (Ig), dysgranular (Id) and agranular (Ia) subdivisions. Filled red circles in section 1 depict locations of VENs neurons. The positions of the sections on lateral view of the insula block and method for unfolding the insula are illustrated in upper panels. Cytoarchitectonic subdivisions encountered at middle level of the insula (coronal section and unfolded map, middle and right panels) are depicted by blue symbols of graded intensity. A dotted green line in middle section indicates contour of layer IV. In the unfolded map, only major sulci and gyri are represented, with the SPS used as reference. See list of abbreviations and the Methods section for details of the graphical reconstruction.

RESULTS

Cytoarchitectonic organization

According to similar criteria as in monkeys, seven cytoarchitectonic subdivisions (G, Ig, Id1-Id3, Ia1-Ia2) were recognized in the human insula. The distinctive features (granularity, i.e. density and width of layers II and IV; morphology and sublaminar distribution of pyramidal neurons in layers III and V) are summarized in Table 2 and illustrated by photomicrographs in Fig. 2. The most dorsal and posterior part of the insula is typified by ''hypergranular '' appearance (G field) with characteristics similar to neighboring cortex in posterior parietal and temporal opercula, including the retroinsular area (RI) posterior to the insula at the junction between parietal and temporal opercula in the Sylvian fissure. The rest of the insula is characterized by progressively decreasing density and thickness of granular layers II and IV, from Ig to Id1, until the disappearance of granular cells in Ia1/Ia2. The size and density of pyramidal neurons also varied across the insula, with an increase of layer V neurons in dysgranular and agranular fields. The presence of numerous VENs (particularly in Ia2) gives a distinctive columnar arrangement in the agranular insula (Figs. 2 and 8). These neurons were plotted under high-magnification and identified according to morphological criteria described by others, i.e. large fusiform, bipolar neurons (see microphotographs in Figs. 2, 5 and 8). They were localized mainly in layer V, but few were also found in layer III. Their distribution (filled circles in sections of the anterior insula in Figs. 1, 2, 5 and 8) was the densest in agranular cortex (anterior part of Ia2) and in adjacent OFC but numerous were also found in dysgranular cortex, in anterior parts of Id1 and Id2 (see photomicrographs Figs. 2 and 8).

Unfolded maps. In order to compare the insular subdivisions and their relative surfaces, the different cytoarchitectonic subdivisions were first represented on unfolded maps of the insula, using similar approach as in monkeys (Gallay et al., 2012). The results for the two most complete maps reconstructed from coronal sections are illustrated in Figs. 3 and 4, with the horizontal lines representing the fundus of the SPS as reference. One map (Hb3-R, Fig. 4) extends more anteriorly than the other, including small part of adjoining orbitofrontal operculum. In the case of Hb2-L (Fig. 3), a 4-mm gap between 2 tissue blocks is indicated by dotted lines along the postcentral insular

sulcus (PIS) and the IPS. The areas were filled with granular (Ig) type by extrapolation with more posterior and anterior sections. The two maps exhibit similar overall organization: granular domain (G and Ig) occupies dorsal and posterior aspects of the insula, overlapping with dorsal and posterior parts of the posterior long insular gyrus (plg), dorsal anterior long insular gyrus (alg), posterior short insular gyrus (psg) and for Ig, also part of middle short insular gyrus (msg) and anterior short insular gyrus (asg). Dysgranular domain encompasses all gyri, in a dorsal to ventral gradient from Id3 to Id1, and the agranular domain (Ia1 and Ia2) covers ventral and anterior aspects of the insula, extending from the ventral alg to the annectant gyrus (ag). A near concentric organization is apparent in both cases but is more conspicuous in the case of Hb3-R where the map extends into posterior part of the OFC. In both maps, contour lines for the different subdivisions are irregular, with steep changes often corresponding to the unfolding of cortex lying deep into sulci. One important feature seen on unfolded maps Hb2-L and Hb3-R is the reversal of gradients that occurs at the junction with the temporal lobe, near or within the IPS in the middle insula, and anteriorly, at the junction with OFC (Figs. 3 and 4).

A similar cytoarchitectonic pattern is seen in the unfolded map reconstructed from horizontal sections (Fig. 9), although the map does not extend as far dorsally and ventrally as the other two. Because of the orientation of sections, the largest variations occur along the anteroposterior axis, with the map particularly ''stretched'' at middle level where the sections cut through all major sulci. Nevertheless, the cytoarchitectonic subdivisions are arranged similarly to the other two maps, with progression from granular to dysgranular and agranular cortices in a postero-dorsal to antero-ventral direction.

In order to evaluate the proportions of major cytoarchitectonic domains (G, Ig, Id and Ia), surface areas were measured in the two most complete cases reconstructed from coronal sections. For comparison, the surface comprised between the SPS, dorsally, the IPS (or its medial limb, IPS-m) ventrally, and near the limit with OFC anteriorly, was taken as demarcation of the insula per se (Ture et al., 1999). Thus for the map of Hb3-R which is more extensive than that of Hb2-L, the anterior limit was placed at the junction with the orbitofrontal operculum, i.e. at the margin with the transverse insular gyrus (tg) (interrupted vertical line in

Table 2. Cytoarchitectonic characteristics of insular subdivisions

|	
G	Dense and broad granular layers II and IV; sublamination layer III with larger pyramidal cells deeper, near layer IV; sparser and smaller cells in layer V; clear separation layers IV/V and V/VI
Ig	Similar to ''G'', but slightly thinner layers II and IV, and larger pyramidal cells in layer V
Id3	Progressive decrease of layers II and IV thickness; sublamination layer III; superficial layer V pyramidal cells pervading into layer IV; no clear separation V/VI
Id2	Similar to Id3, but sparser and thinner layers II and IV; smaller cells and blurred sublamination layer III; few VENs in layer V
Id1	Similar to Id2, but faint granular layer IV; large pyramidal cells in layer V; presence of VENs anteriorly
Ia2	Disappearance of granular cells; pronounced vertical arrangement of neurons in layers III and V; numerous VENs in layer V (few also scattered in layer III)
Ia1	Broad fused layers II/III and V/VI; only few VENs
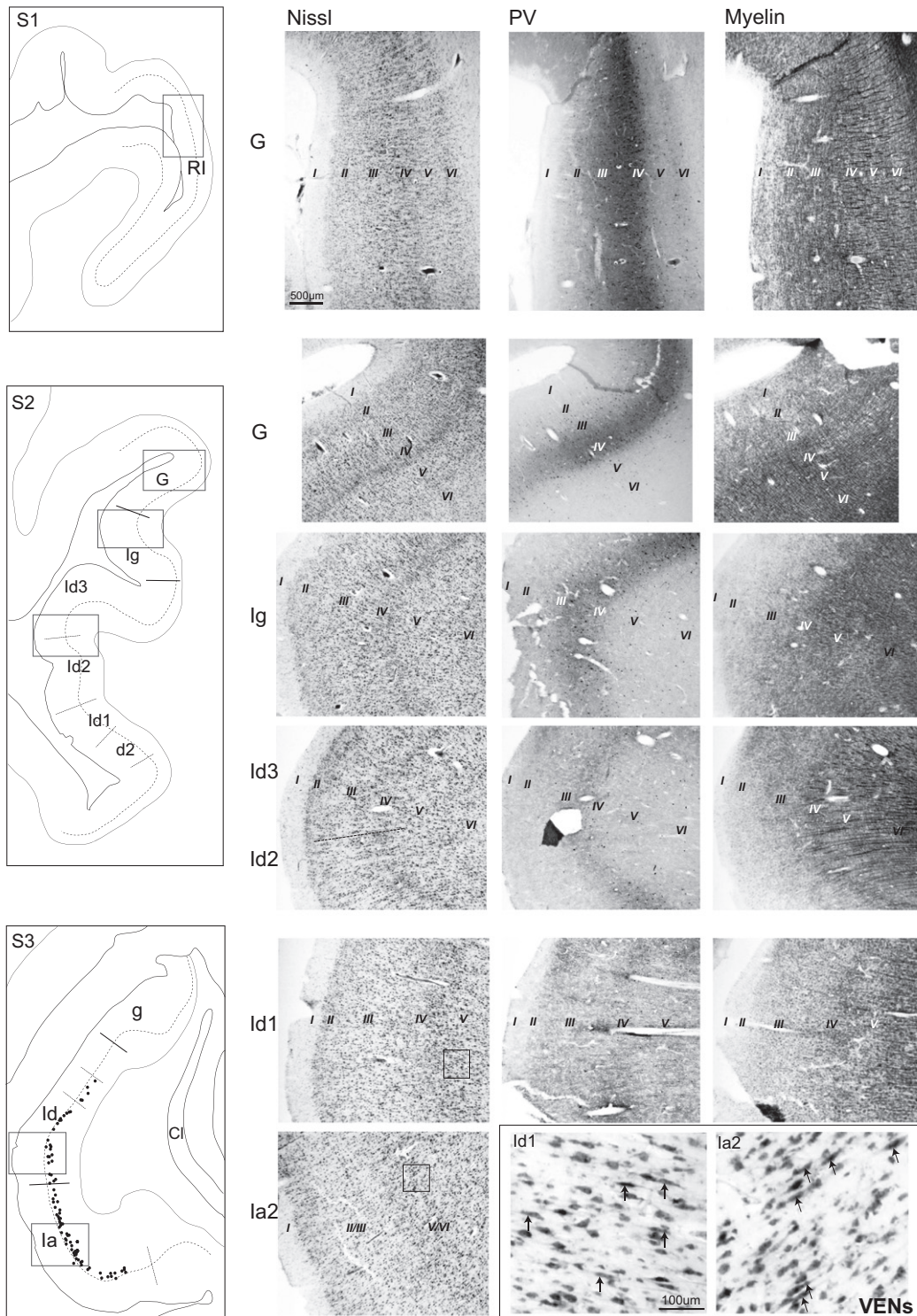
Fig. 2. Patterns of intracortical Nissl, PV and myelin in the insular subdivisions. Photomicrographs were taken from adjacent coronal sections at levels indicated on drawings of the corresponding sections in the left panels. Lower right photomicrographs: higher magnification of VENs neurons (pointed arrows) in dysgranular and agranular insula, in areas enclosed in small rectangles. Sections 1–3 correspond to Sections 6, 3 and close to 1 of Fig. 1. Filled black circles in S3 represent the distribution of VENS. See list of abbreviations.

Fig. 4). This limit also corresponds to reversal of the cytoarchitectonic gradients. The total insular surface was similar in the 2 cases, varying between 5'300 mm^2 for Hb2-L and 5'070 mm^2 for Hb3-R (not corrected for shrinkage). The proportions of the different cytoarchitectonic domains were 23% (18%) for G, 20% (15%) for Ig, 47% (55%) for Id and 10% (12%) for Ia in Hb2-L (respectively in Hb3-R). The dysgranular domain
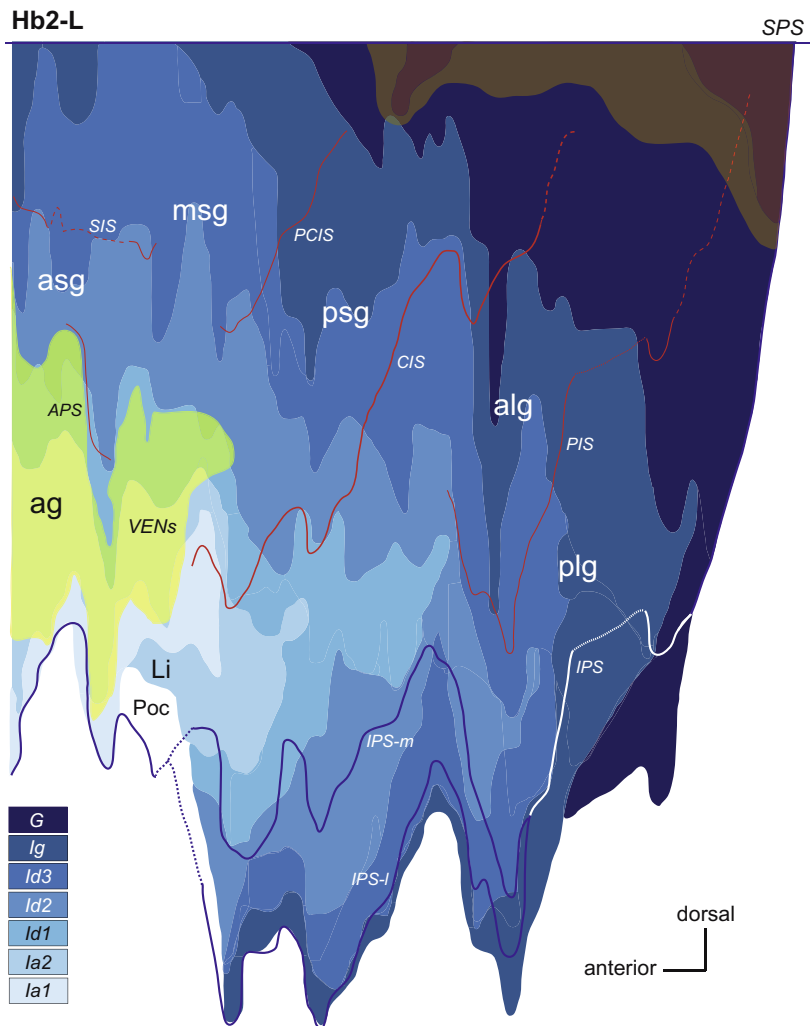
Fig. 3. Unfolded map of the insula in the case of Hb2-L. Cytoarchitectonic subdivisions are represented by graded blue areas (color codes indicated in lower left). The horizontal straight line represents the reference SPS. Major sulci separating insular gyri are shown in red and the peri-insular sulci (IPS, IPS-m and IPS-l) are depicted in dark blue or white. Interrupted or dotted lines along sulci relate to dimming of the sulcus or extrapolation due to intervals between tissue blocks, respectively. The dorsal and posterior area in dark red designates the zone of densest PV neuropil in middle layers, and the area in yellow represents the distribution of VENs. See list of abbreviations.

occupies the largest surface in both maps and this is also apparent in the case of Hb4-L (Fig. 9). However in the latter case, no quantitative comparison could be made since the map only partially covered the insula explored in Hb2-L and Hb3-R.

Localization of VENs. The distribution of VENs is represented by yellow areas in the unfolded maps of Figs. 3, 4 and 9. These delimitations correspond to zones of relatively dense accumulations of VENs and do not include regions of sparse and scattered distributions. In all 3 cases, the density of VENs was the highest in most anterior part of the insula, encompassing the anterior short and accessory gyri (see also Fig. 7). Their distribution was not confined to the agranular domain, but clearly extended into neighboring dysgranular fields Id1 and Id2 (only rare in Id3). Proportions of VENs areas overlapping with dysgranular versus agranular fields were estimated 41% and 32%, in the cases of Hb2-L and Hb3-R, respectively.

Myeloarchitecture

The staining of myelin with the Black-Gold II method provided additional criteria for evaluating architectonic organization of the insula. Changes from radial, densely packed intracortical myelinated fibers in dorsal and posterior insula, to progressively decrease, especially in superficial layers, toward antero-ventral insula follow overall cytoarchitectonic gradients. The clear demarcation of an outer band of Baillarger (BB) is recognized in Ig and dysgranular fields Id3 and Id2, but disappears in Id1 and in agranular insula where myelin is relatively weak, except in deep layers (Figs. 1, 2 and 6). A strong layer I plexus delimits the medial border of the agranular insula with Poc in most anterior sections (e.g. S1, Fig. 1). Important to notice the strong myelination in parietal operculum and in posterior superior temporal plane (e.g. in Heschl's gyrus (HG)), as well as progressive appearance of the outer BB along the temporal operculum, starting near the IPS-l
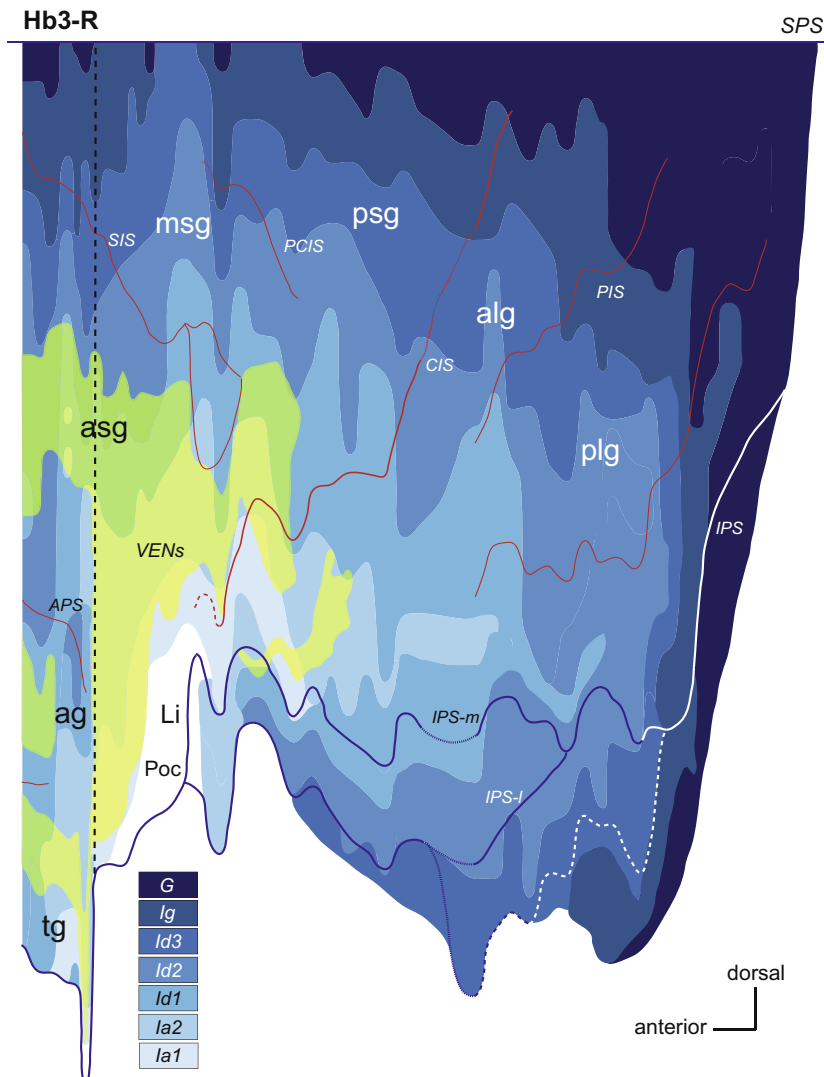
Fig. 4. Unfolded map of the insula in the case of Hb3-R. The left vertical interrupted line indicates the anterior limit corresponding to the insula mapped in Fig. 3. The interrupted white line below IPS-l corresponds to the limit with HG. Same conventions as in Fig. 3. See list of abbreviations.

(e.g. S3, Fig. 1). Because of uneven and often weak staining, the borders were difficult to assess, particularly in anterior insula, thus precluding similar detailed representation as for the Nissl unfolded maps.

Parvalbumin

Immunostaining for PV was light and often inhomogeneous in central and ventral parts of the insula. However, a zone of marked neuropil staining in middle layers was identified in all cases in dorsal and in posterior insula (Figs. 1 and 2 and red area in Fig. 3), coinciding largely with "G" cortex. Interestingly, a region of particularly strong PV is seen in middle-dorsal insula, at level of the psg. Staining in layers III–IV is also clearly visible in Ig, but decreases progressively in intensity in Id3 and Id2, to become nearly undetectable in Id1 and Ia (Figs. 1 and 2). In parallel to the high intracortical myeloarchitecture, a strong PV immunostaining in middle layers characterizes RI and

regions in posterior parietal and temporal opercula, particularly in HG.

MRI projections

In three cases (Hb2, Hb3 and Hb4, Table 1) cytoarchitectonic maps were registered to postmortem MRI following a procedure described in the Method section and illustrated for the case of Hb3-R in Fig. 6. Correlations of Nissl and myelin sections with corresponding coronal MRI are also illustrated in Fig. 5. The overall topographic anatomy of the insula seen in MRI is comparable between the 3 cases, with five well recognizable gyri and sulci. The gyri differ in size and orientation (especially in mid-anterior insula) and an additional sulcus divides the plg in the case of Hb3-R and the asg in the case of Hb4-L. The least prominent gyrus is the msg, particularly in the case of Hb4-L where it is visible only on most medial sagittal MRI.

The projections of cytoarchitectonic maps onto sagittal MRI are illustrated in Figs. 7 and 9. The position of sagittal
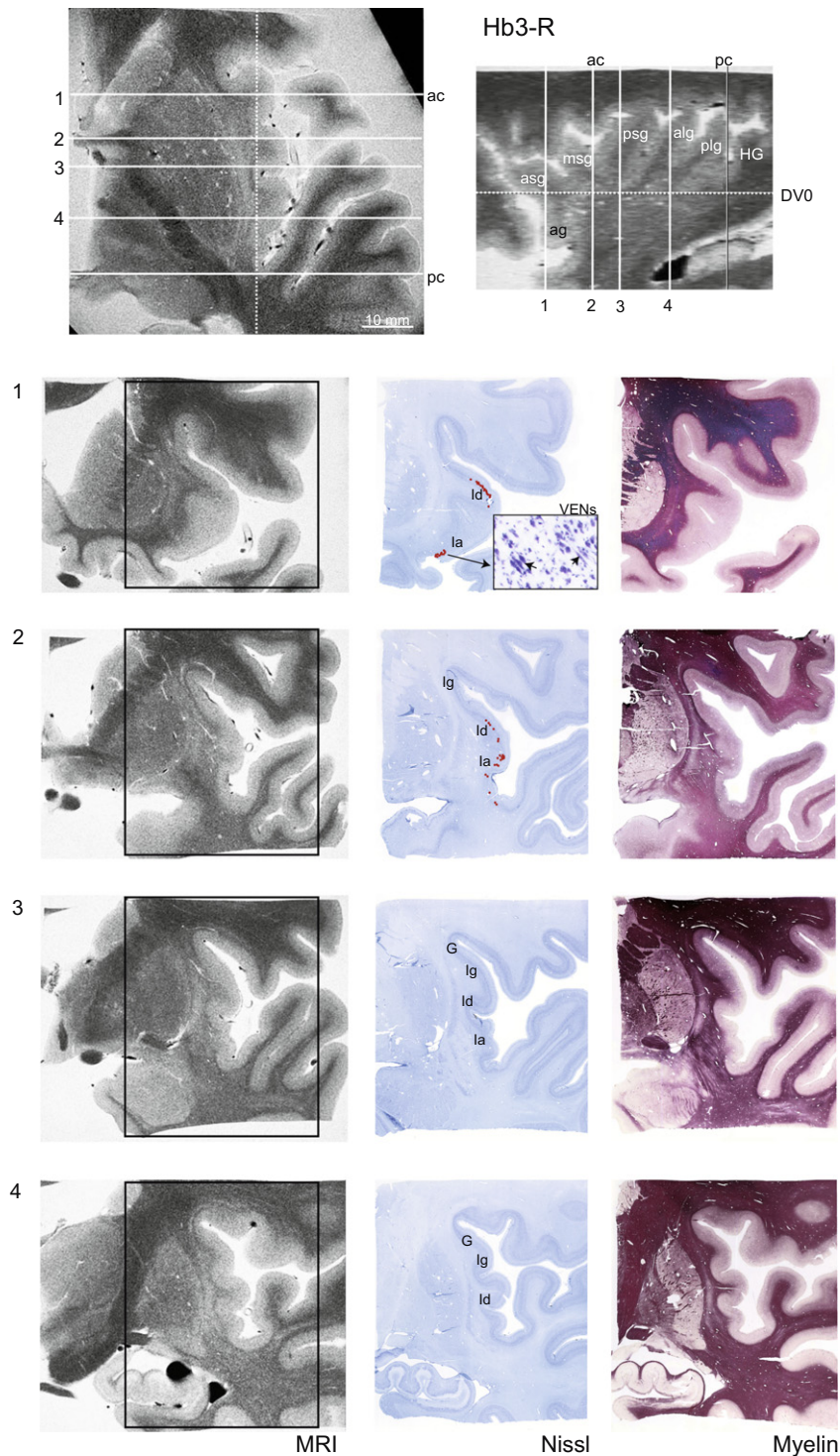
Fig. 5. MRI correlations with histology. Series of anterior to posterior (from top to bottom) coronal 3T postmortem MRI (left column) and closest sections of the insula block stained for Nissl and myelin. The areas enclosed by the histological sections are demarcated by black rectangles in MRI. Coronal levels and positions of stereotactic planes are depicted on horizontal and sagittal MRI in upper panels. The major insular subdivisions and distribution of VENs (filled red circles) are indicated on Nissl series. A small inset in section 1 displays VENs neurons in agranular (Ia) insula. See list of abbreviations.

planes is indicated in insets (on miniature horizontal MRI). In each case, a first map (labeled sag 1) represents the surface projections of cytoarchitectonic subdivisions onto a medial sagittal MRI through the largest part of the

insula. This was performed to generate a surface representation in relation to MRI insular morphology. In more lateral planes, only cytoarchitectonic segments intersecting with grey matter are projected, giving rise to
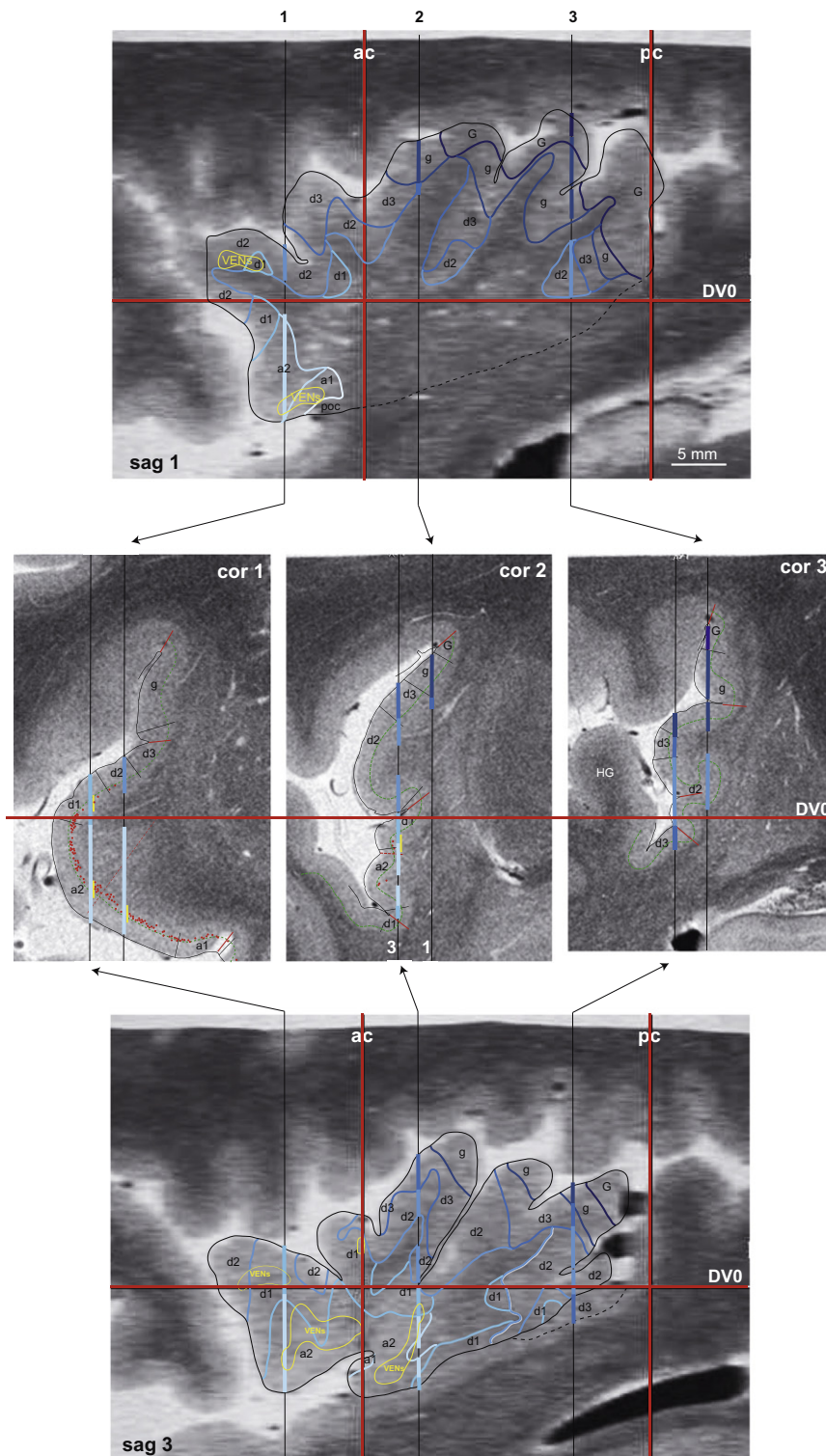
Fig. 6. Procedure for sagittal MRI registration. Neurolucida plots of insular cytoarchitectonic borders (case Hb3-R) are projected onto corresponding coronal MRI (middle panels) where the position of planes corresponding to the sagittal medial (sag 1, upper panel) and lateral MRI (sag 3, lower panel) are represented by the two vertical lines. Colored segments (see color codes in Figs. 3 and 4) correspond to cytoarchitectonic subdivisions encountered in the grey matter. Positions of stereotactic planes are indicated by horizontal (DV0) and vertical (ac and pc) red lines. VENs distributions are represented by filled red circles in coronal section 1, and outlined by the yellow area in sagittal MRI reconstructions. See list of abbreviations.

partially filled maps differing according to topographical anatomy of the insula in the 3 cases. As observed in the most complete cases (Hb2-L and Hb3-R, Fig. 7), the

gradients are oriented obliquely, almost orthogonal to the axes of the long insular gyri in posterior insula, and become more horizontally oriented in middle and anterior
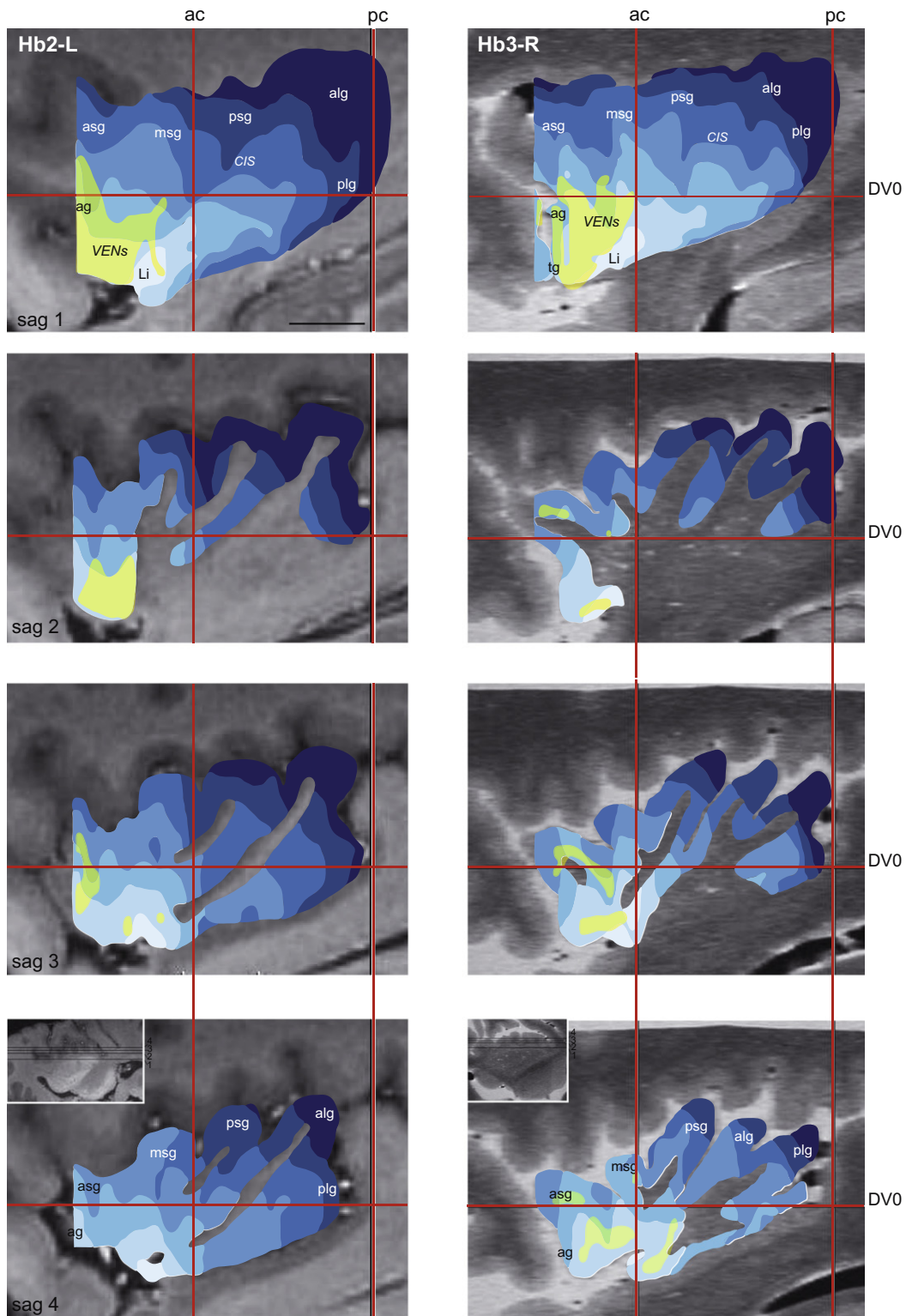
Fig. 7. Sagittal MRI registrations of maps Hb2-L and Hb3-R. The cytoarchitectonic maps are registered to sagittal MRI (see levels in inset horizontal MRI in lower panels) and arranged from medial to lateral (sag 2–4). The distance between sagittal MRI 2–4 is smaller (1.5 mm) in the case of Hb3-R than in the case of Hb2-L (2.5 mm). A surface map projected onto more medial MRI (sag 1, upper panels) gives the full extent of the cytoarchitectonic subdivisions in relation to sulcal/gyral insular landmarks. Stereotactic planes are indicated in red. Scale bar (upper left panel) = 10 mm. Same color codes as in Figs. 3, 4 and 6. See list of abbreviations.

insula. Each cytoarchitectonic domain expands across several gyri: the granular domains (G and Ig) form a more or less continuous band across dorsal and posterior parts

of the plg, dorsal part of the alg, psg and for Ig, also part of msg. A separate strip of Ig is also present in dorsal asg. The dysgranular subdivisions encompass all gyri, in
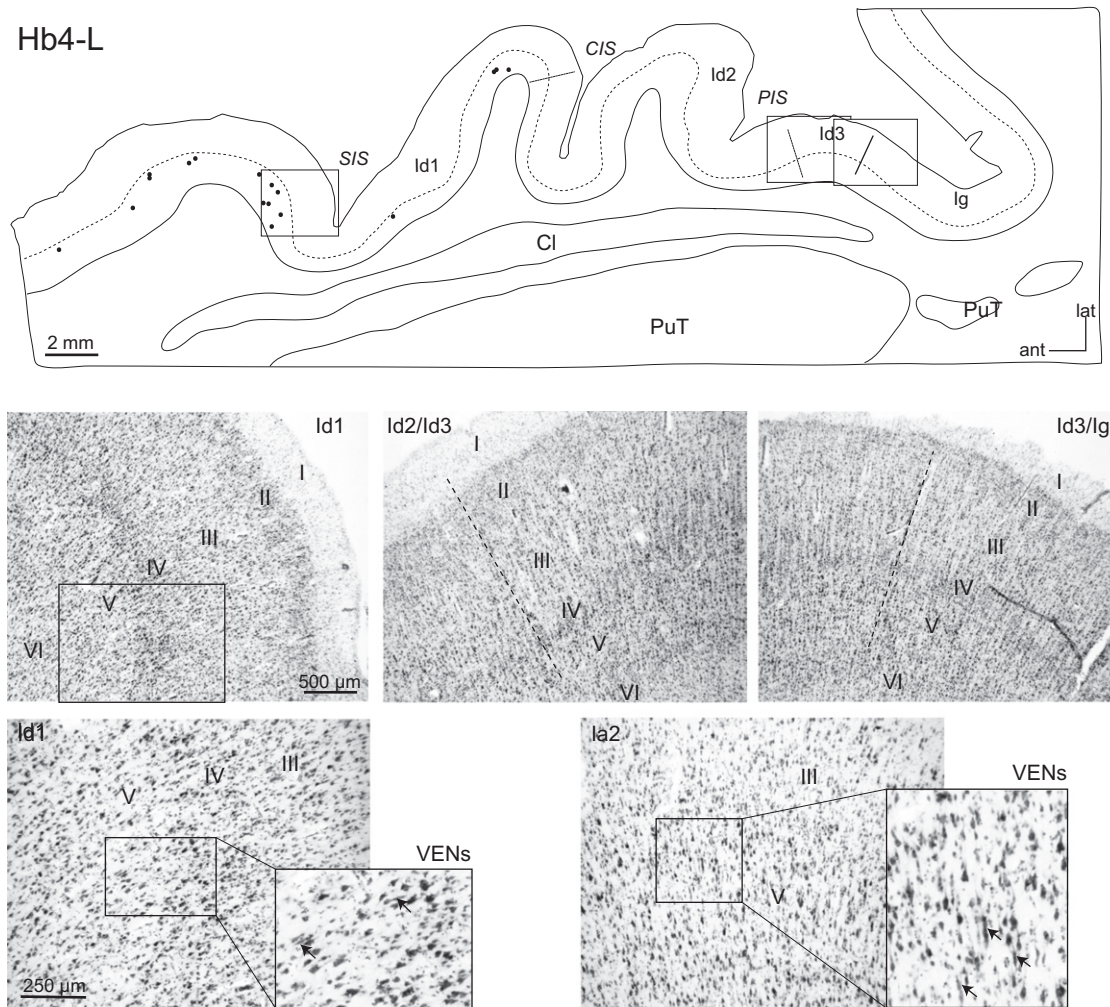
Fig. 8. Cytoarchitectonic patterns in the horizontal section. The section (drawing in upper panel) is at intermediate dorso-ventral level of the insula. Filled black circles represent the distribution of VENs. Photomicrographs illustrate progressive thickening of layers II and IV from Id1 to Ig (first row), and higher magnifications of part of Id1 to show the faint layer IV and presence of few VENs (lower left panels). The typical appearance of Ia2 with numerous VENs is illustrated by a photomicrograph at more ventral levels of the insula (lower right panels). See list of abbreviations.

a dorsal to ventral gradient from Id3 to Id1. In the agranular insula, Ia2 stretches from the ventral alg to the < ag while Ia1 is mainly restricted to the Li, at the ventral tip of the long gyri. As already apparent in unfolded maps, there is a concentric-like arrangement of the gradients around the Poc and Li, which is particularly obvious in the case of Hb3-R where the map extends beyond the insula, into posterior OFC. The major part of the VENs areas, best represented on surface projections maps, lies over Ia2 on the ag, with some extension into dysgranular domain on the asg and tg (case Hb3-R). The same tendency is observed in the case of Hb4-L (Fig. 9), although the map is incomplete in the most dorsal and ventral insula.

The MRI maps were reconstructed in stereotactic planes represented by the reference intercommissural line, DV0 (= ac–pc), passing through the centers of the anterior (ac) and posterior (pc) commissures, and the coronal ac and pc planes orthogonal to DV0. Despite differences in brain morphology (cortical atrophy and smaller insula map in the case of Hb3-R) and different ac-pc distances (24, 26 and 27 mm in the cases of Hb2-L, Hb3-R and Hb4-L, respectively), the positions of the

stereotactic planes in relation to insular morphology and cytoarchitectonic maps did not differ significantly. The ac plane intersected with the posterior margin of the msg in the cases of Hb2-L and Hb3-R, and middle msg in Hb4-L (Fig. 9), while the pc plane was positioned around the postero-dorsal limit of the long gyri in the cases of Hb2-L and Hb3-R and slightly more anterior in the case of Hb4-L. The horizontal DV0 plane crossed approximately through the middle dorso-ventral extent of the insula, from the posteroinferior angle defined by Afif and coll. (Afif et al., 2009) as situated between the inferior and posterior peri-insular sulci, to near the ventral limit of the asg with ag. This plane lies slightly more dorsal relative to insular gyral/sulcal anatomy in the case of Hb4-L (Fig. 9).

DISCUSSION

Major findings

(1) Unfolded maps of the insula confirm overall cytoarchitectonic gradients proposed by Mesulam (Mesulam and Mufson, 1985): from postero-dorsal
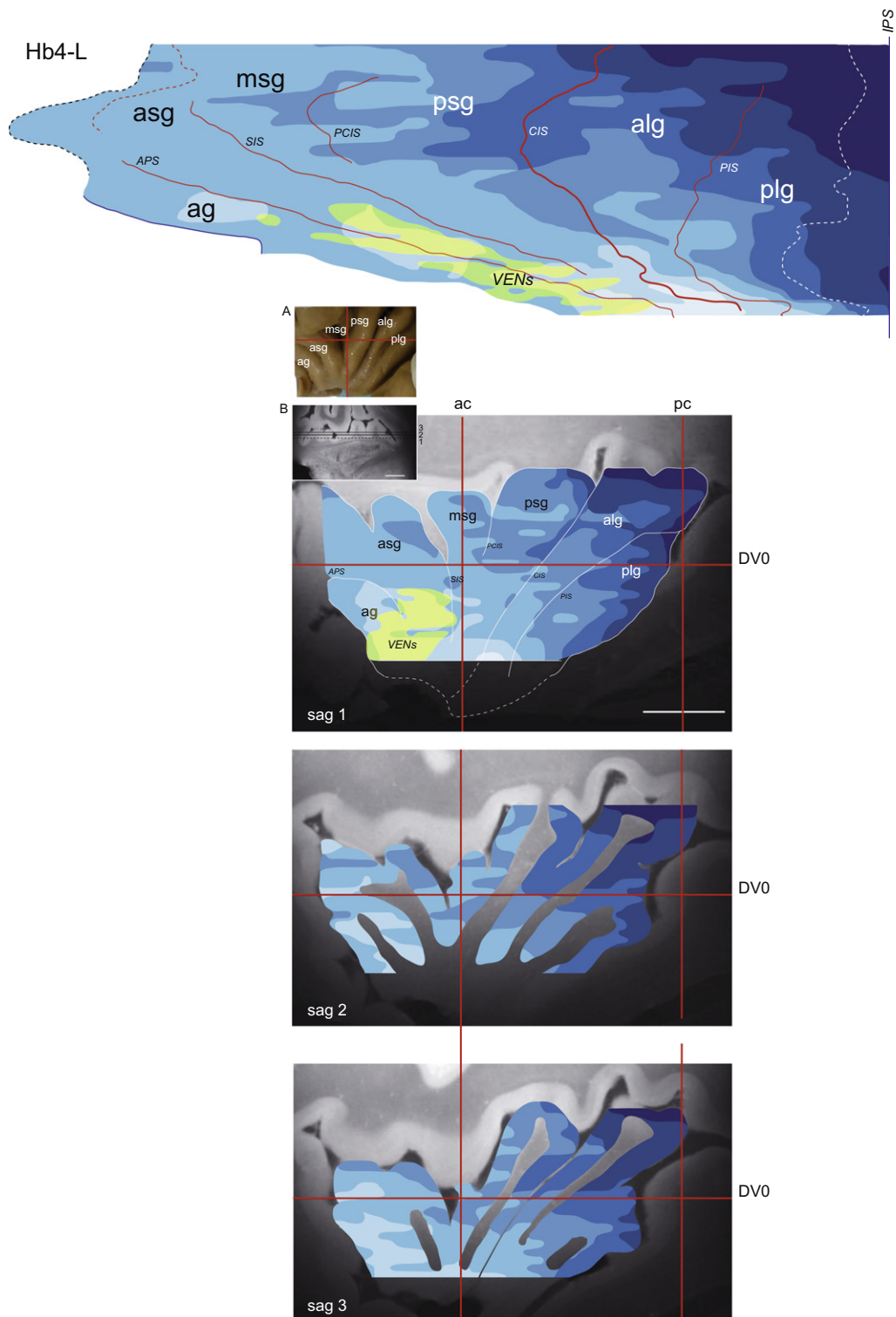
Fig. 9. Unfolded map and MRI projections of the case of Hb4-L. The insula was cut in horizontal sections and the unfolded map (upper panel) is reconstructed from the IPS (reference vertical line) and extends to the anterior border of the block (interrupted blue line) or to the anterior border of ag at more ventral levels. The interrupted white line corresponds to posterior limit of the plg. In sagittal MRI projections (lower panels) the first representation (sag 1) corresponds to surface projections. Small insets show the surface of the insula after moving apart the opercula (A) and the positions of sagittal planes on a horizontal MRI (B). Scale bars = 10 mm. Same conventions as in Fig. 7.

granular cortex, to middle dysgranular and antero-ventral agranular cortex. The dysgranular domain occupies the largest insular territory (about half of the total surface).

(2) Reversals in cytoarchitectonic gradients occur at the junction with the temporal operculum (pointing to a limit with auditory cortex) and in the anterior insula, at the border with OFC.

(3) Distribution of VENs in the anterior insula is most important in the agranular domain, but significant numbers are also localized in dysgranular fields.

(4) Projections of cytoarchitectonic maps onto sagittal MRI demonstrate that each major domain extends across several insular gyri, with the largest territory devoted to dysgranular domain spreading over all gyri.

(5) The position of stereotactic planes in relation to topographical gyral and sulcal patterns is quite comparable across cases in spite of difference in overall brain morphology.

Methodological considerations

Our anatomical study is based on a small number of specimens (4 hemispheres from 4 brains) that had different fixation durations and for two of them, no information was available on age, gender, cause of death and postmortem delays. Postmortem MRI scanning confirmed that there were no major pathological signs in the hemisphere under study. Three specimens included a major part of the insula that was mapped in detail according to cytoarchitectonic transitions, and to lesser extent also, to changes in myeloarchitecture and PV immunostaining. Our approach was a "classical" one, i.e. determination of architectonic borders under microscopic examination. This approach, which we used recently for the monkey's insula (Gallay et al., 2012), also allows best comparison with previous maps of the human insula, especially those following Mesulam's scheme of insular cytoarchitectonic organization (Mesulam and Mufson, 1985; Bonthius et al., 2005). This approach however is very time-consuming and cannot easily be applied to a large number of specimens, which impedes quantitative evaluation of inter-individual, gender or hemispheric variations. Recently, new methods were developed to apply "observer-independent" analysis of cytoarchitectonic delimitations on a large number of specimens and provide 3D MRI templates and probabilistic maps for neuroimaging (Amunts and Zilles, 2001; Morosan et al., 2005; Schleicher et al., 2005; Eickhoff et al., 2006b; Mackey and Petrides, 2009). The method has been applied to several cortical areas, including the posterior insula with probabilistic maps of granular, dysgranular and agranular subdivisions (Kurth et al., 2010b). Whereas this quantitative approach is currently the only one to provide 3D representations of cortical areas for integration into a standard 3D MRI template of the human brain (e.g. MNI atlas), the accurate detection of architectonic boundaries is still subjected to several variables, such as irregular or low-contrast staining, cortical folding, planes of sections tangential to gyral surface, gradual more than sharp architectonic transitions. These problems also influence detection and positioning of borders under microscopic examination but to lesser degree by the use of higher magnification when necessary. Deformations due to formalin inhomogeneous fixation seem to affect to a lesser degree centrally located structures, including the insula (Schulz et al., 2011). More important are deformations occurring during mounting of the sections but these remain relatively small in the insula in comparison to the opercular cortex. The shrinkage due to staining on mounted sections (Nissl and myelin) was relatively small (6% by projections of scanned images or Neurolucida plots onto postmortem MRI) and not taken into account for reconstructing the unfolded maps.

Architectonic organization

The cytoarchitectonic parcellation was first analyzed on unfolded maps of the insula with a method similar to that used previously for the monkey insula (Gallay et al., 2012). This procedure applied to the human insula provides more direct comparison with the monkey's insular cytoarchitectonic organization and with the few, more "conventional" maps of the human insula. The number of cytoarchitectonic subdivisions (7) was determined according to similar criteria used to define subdivisions in monkeys, except for the granular insula (Ig) where no separate subsectors could be firmly identified. The hypergranular field "G" has characteristics comparable to the cortex on adjoining parietal and temporal opercular areas, although less differentiated than in primary sensory areas such as AI on HG. The irregularity of the contours for the different cytoarchitectonic subdivisions is quite marked, more than in monkeys, and is largely due to the complex sulcal/gyral morphology of the human insula. Unevenness is also related to the difficulty to detect reliably borders in depth of sulci or in portions of the cortex cut tangentially.

A number of cytoarchitectonic parcellations have been proposed in the past for the human insula (see for review (Nieuwenhuys, 2012a), but the architectonic scheme developed by Mesulam and Mufson (1985) still represents the fondement for current studies of the insula. The cytoarchitectonic gradients seen in our unfolded maps follow the same general orientation and organization as proposed by Mesulam on the basis of comparable observations as in monkeys. Related to insular gyral/sulcal landmarks, the map corresponds to that of (Bonthius et al., 2005) where each cytoarchitectonic domain encompasses several major gyri and sulci. It differs however from a recent probabilistic map of the posterior insula (Kurth et al., 2010b) where the granular domain remains posterior to the CIS. The present maps extend beyond the peri-insular (or circular) sulcus and demonstrate several reversals that point to the transition between the insula and auditory cortex in the temporal operculum, and between the anterior insula and OFC (seen in the case of Hb3-R, Fig. 4). The cytoarchitectonic transition with auditory cortex corresponds approximately to the lateral boundary of pro-isocortical or temporoinsular areas described before (Galaburda and Sanides, 1980; Morosan et al., 2001; Chiry et al., 2003; Fullerton and Pandya, 2007). In previous anatomical study of the orbital and medial prefrontal cortex, the most anterior insula was characterized as agranular and subdivided into four different architectonic areas (Ongur et al., 2003). Their area Ial located in the dorsal anterior insula

and corresponding to part of FI (Von Economo, 2009; Allman et al., 2010) is most differentiated in the Nissl and myelin sections. Because of faint, but increasingly visible layer IV towards SPS (see Fig. 2), as well as relatively dense myelination, we included this region in the dysgranular insula.

The surface of the insula was similar in the two cases and is nearly three times that of the monkeys (5 cm^2 versus 1.9 cm^2), in a similar ratio to that reported recently (Nieuwenhuys, 2012a). This value is in the range (3.4–7.1 cm^2) given by Rivier and Clarke (Rivier and Clarke, 1997) in the four hemispheres they have analyzed. The relative proportions of the cytoarchitectonic domains were compared with those measured in unfolded maps of the monkey's insula (Gallay et al., 2012). The major difference is that dysgranular (Id) domain in average represents half the anatomical territory in the human insula, versus a third in the monkey. The granular (G and Ig) are reduced, and agranular increased (by about twofold) in the human insula compared to monkeys. The particular increase in dysgranular domain in the human insula has to be related to the large expansion of multimodal, associative cortex and their interactions with the insula.

The relation of cytoarchitectonic parcellation with myeloarchitecture and PV immunostaining was similar to that in monkeys, although the analysis was less detailed due to the lower quality of brain tissue and staining. The changes from strong intracortical myelin in the dorsal and posterior insula, to progressively lighter myelination towards the ventral and anterior insula are consistent with gradients observed previously (Mesulam and Mufson, 1982a, 1985; Ongur et al., 2003; Gallay et al., 2012). Both Ig and Id (Id3–Id2) were characterized by an outer BB which decreased in intensity from Ig to Id2. This outer BB was not clearly separated in G because of the density of intracortical myelination, as was also the case in the posterior parietal and temporal opercula. The myeloarchitectonic gradients differ in orientation from earlier parcellations reported in a recent review on myeloarchitectonic studies of the human cerebral cortex (Nieuwenhuys, 2012b). The immnostaining for PV, although not optimal for mapping the entire insula as in monkeys, provided additional criteria for delimitations in the posterior and dorsal insula. Zones of PV-rich fiber plexuses in middle layers coincide largely with the G cytoarchitectonic domain. Interestingly, the zone of densest PV (see Fig. 3) is discontinuous in dorsal insula, with a separate area at mid-dorsal level (overlapping with the dorsal psg). This area has been associated with sensory processing, in particular pain, but is also considered as primary human taste area (Small, 2010). Stimulations of this region evoked viscerosensations, including gustation (Stephani et al., 2011). It resembles the PV-rich area in the anterior insula of the monkey and the "shift" to more posterior locations in humans was suggested to be related to the specific development of the anterior insula. Neuroimaging studies show quite different activation patterns depending on the taste stimulus, but the sensitivity of this presumed primary

taste area to oral touch, texture and temperature goes along with a more "sensory", thalamic afferented hypergranular and PV dense cortex as is the case in our study.

Reversal observed at the temporal opercular side with the cytoarchitecture is also seen with myelin and PV stainings. The approximate insulo-auditory boundaries correspond to immunohistochemical transitions observed by others medial and anterior to HG, near the IPS (Rivier and Clarke, 1997; Chiry et al., 2003).

VENs areas

The majority of VENs were found in the anterior insula, in the region designated as FI. Since the early description by Von Economo (Von Economo and Koshinas, 1925; Von Economo, 2009), the distribution of VENs has been examined in detail in a number of species and found in both the insula and the anterior cingulate cortex (ACC) (Nimchinsky et al., 1995; Allman et al., 2010; Butti and Hof, 2010). Von Economo neurons were long thought to be present only in the agranular insula of great apes and humans, although a recent study described them also in anterior FI of macaque monkeys (Evrard et al., 2012). Our data confirm the overall distribution of VENs in the anterior insula, but demonstrate in addition that these neurons occupy a fairly large territory covering part of the agranular domain but also extending into dysgranular fields (Id1 and Id2). The presence of VENs in Id may have a role in strengthening cognitive-emotional interactions in humans. The larger size of the agranular domain and more extensive distribution of VENs in the human insula compared to monkey suggests, as proposed recently (Nieuwenhuys, 2012a), that the human anterior insula has expanded and "specialized", rather than being a "newly evolved" area unique to hominoids. No obvious lateralization was found in the distribution of VENs, since similar distributions were observed in left (Hb2-L and Hb4-L) and right (Hb3-R) hemispheres. More quantitative analysis, on a larger sample is necessary to uncover inter-hemispheric differences, such as for a right hemisphere dominance emphasized by others (Allman et al., 2011).

The VENs in anterior insula and ACC, which are two closely interconnected paralimbic areas, are proposed to be important in a neural circuitry underlying social awareness (Allman et al., 2005). Indeed, loss of VENs and dymorphies have been found in fronto-temporal dementia (FTD) which is a clinic syndrome affecting social awareness, self-control and empathy. The association between VENS density differences or morphological anomalies has also been studied in several neuropsychiatric disorders including autism, agenesis of the corpus callosum as well as in schizophrenia (Simms et al., 2009; Seeley, 2010; Butti et al., 2013; Santos et al., 2011). However, most analyses were carried out in the ACC and only a few in the insula.

MRI correlations

The projections of cytoarchitectonic maps onto postmortem MRI aim at providing an anatomical basis for later developments and applications in neuroimaging. Direct visualization of microstructural changes in MRI was not possible (or at least too unreliable) at the level of the insula for direct correlation between MR and cyto- or myeloarchitectonic maps. Recent studies used high-resolution MRI (postmortem and *in vivo*) to detect changes corresponding to architectonic boundaries mapped from histological preparations, principally myeloarchitecture (Fatterpekar et al., 2002; Walters et al., 2003; Eickhoff et al., 2005; Blaizot et al., 2010; Geyer et al., 2011). These correlations are most reliable in koniocortical areas (e.g. primary visual, auditory and somatosensory cortices) where myelination is very dense across cortical layers, but more difficult to obtain in more distant, less myelinated areas including the insula. Nevertheless, a recent myelin-based *in vivo* MRI study (Glasser and Van Essen, 2011) reports that myelin content in the insula enables differentiation between granular, dysgranular and agranular domains, but not between subdivisions within Ig or Id of the probabilistic maps of Kurth et al. (2010b).

Projections onto sagittal MRI indicate that the gradients run nearly orthogonal to the orientation of CIS and the long gyri, similar to a map adapted from Mesulam by Anderson et al. (2009) and to the topographic representation by Bonthius et al. (2005). In all, each major cytoarchitectonic domain expands across several major gyri, with the dysgranular field across all. The Ig extends beyond the CIS, in dorsal portions of psg and msg, in contrast to the recent probabilistic map of the posterior insula (Kurth et al., 2010b) where it remains posterior to CIS. Taking into account that subdivisions in the probabilistic map are numbered inversely to those in the present report, discontinuities appear such as in dorsal insula between granular Ig2 and putative Id3 corresponding to the least differentiated dysgranular field (see the flatmap in their Fig. 5). Such discontinuities were not seen in our maps, nor did they occur in previous cytoarchitectonic parcellations of the insula in the macaque monkey (Gallay et al., 2012). The difference is most likely related to the different methods used for detecting borders. Complementary multiarchitectonic approach, as used in the human auditory cortex (Wallace et al., 2002; Chiry et al., 2003; Morosan et al., 2005), and correlations with digitally produced maps will help refine the human insular parcellation for neuroimaging applications.

Relation to cortical connectivity

The importance of connectivity in understanding cortical organization and function is reflected by the profuse literature based on animal tracing experiments. In the monkey insula, major cytoarchitectonic subdivisions were differentiated by their patterns of connections with a number of brain areas and an antero-ventral to postero-dorsal gradual, more than strict, topographical

organization (Mesulam and Mufson, 1982b; Mufson and Mesulam, 1982, 1984; Augustine, 1985; Friedman and Murray, 1986; Friedman et al., 1986). In the human brain, the recent possibility to explore *in vivo* structural and functional connectivity has been increasingly attractive and applied to study insular functional organization (Cauda et al., 2011; Cerliani et al., 2012; Cloutman et al., 2012; Jakab et al., 2012). Though limited by MR image resolution and relatively crude localization of the regions of interest, probabilistic white-matter tractography studies confirm a general olfactocentric antero-posterior organization in the insula, but in addition demonstrate that the region corresponding to Id is more heterogeneously organized than granular or agranular regions and that overall, connectivity patterns of the insula are more gradually organized than in other more specific brain areas such as medial premotor cortex (Cerliani et al., 2012). Resting state functional connectivity also provides evidence for separate ventral anterior and dorsal posterior insula networks underlying emotional and sensorimotor integrations, respectively (Cauda et al., 2011).

MRI variability of the insula and relation to stereotactic space

The number, morphology and topography of insular gyri vary between individuals, especially the anterior small gyri (Ture et al., 1999; Naidich et al., 2004; Afif et al., 2009). However, majority of subjects display five major gyri and this was also the case for our three specimens scanned with MRI. More difference was related to cortical atrophy affecting particularly one brain (Hb3-R) and probably responsible for the reduced size of the insula compared to the others (despite similar or even longer ac-pc distance). The surfaces estimated on MRI (1.2 and 1.4 cm^2 in Hb2-L and Hb3-R, respectively) were in the range of values given in an *in vivo* quantitative MRI analysis by Afif et al. (2009) and represent less than a third (24–26%) of the total surface of the insula measured on unfolded maps. The relation to stereotactic planes was also congruent, taking into account differences of the positions of axes relative to the ac and pc. With the relatively low variability of the insular morphology in relation to stereotactic space, the cytoarchitectonic maps presented on 2D MRI registrations can provide a basis for more accurate anatomo-functional localizations in neuroimaging and MR-guided surgical interventions.

Functional correlations

The diversity of functions (and dysfunctions) attributed to the insular cortex is quite broad and reflected by the long list (at least 20) reported in a recent comprehensive review of the literature (Nieuwenhuys, 2012a). We focus here on functional aspects that have been most thoroughly investigated, i.e. somesthesy and pain. Anatomo-functional correlations mostly derive from invasive pre-surgical diagnostical recordings and stimulations in patients with drug refractory epilepsy

(Ostrowsky et al., 2002; Frot and Mauguiere, 2003; Afif et al., 2008; Mazzola et al., 2009, 2012a; Nguyen et al., 2009; Garcia-Larrea et al., 2010; Stephani et al., 2011). While somatosensory sensations were generally evoked from relatively large portions of the human insula, pain sensations were mostly elicited from stimulations in the middle and posterior dorsal insula, with evidence of crude somatotopy (Mazzola et al., 2009). Lesions in this insular region also result in alterations of thermal and pain sensations, and are likely to induce central pain syndrome (Garcia-Larrea et al., 2010; Veldhuijzen et al., 2010). The mid-posterior dorsal insular region corresponds closely to the territory characterized by granular and hypergranular cortices in the present maps. Interpretation of the data is often limited however in terms of localization due to the difficulty of precisely identifying the location of the electrode tip and to the possible co-activation of adjacent opercular cortical areas, especially the frontoparietal operculum (Pugnaghi et al., 2011). Because of the confounding role of the opercular cortex, the term of operculo-insular cortex for designating areas responsible for pain was particularly appropriate. Using an oblique approach (avoiding passing through the opercula) and 3D imaging, Afif and collaborators (Afif et al., 2008) found that sites inducing pain sensations were confined to the upper portion of the middle short gyrus (while postcentral stimulations evoked painless paresthesias or warm sensations), suggesting a specific role of this insular gyrus in the processing of pain. Accuracy issues concern also functional imaging studies (fMRI, PET) due to their insufficient spatial resolution. Indeed, some of the so-called insular activations clearly involve also the opercular cortex, such as after innocuous thermal stimulation (Craig et al., 2000). Nevertheless, fMRI studies produced congruent results with those of intraoperative stimulations, such as crude somatotopy (Brooks et al., 2005) and a specific activation to pain in the contralateral posterior insula (Mazzola et al., 2012b) and more precisely, in Ig according to correlation with existing probabilistic map (Kurth et al., 2010b). It is important to note that in fMRI studies, single cortical activation is rarely responsible for a function but mostly a group of activations. This also explains different results and interpretations among reports, and the need of further studies using comparable imaging modalities, task-related strategies and anatomical bases.

CONCLUSIONS

This study provides a framework for future complementary multiarchitectonic studies of the human insula and 3D MRI registrations to improve integration into *in vivo* MR imaging and clinical applications.

REFERENCES

Ackermann H, Riecker A (2010) The contribution(s) of the insula to speech production: a review of the clinical and functional imaging literature. Brain Struct Funct 214:419–433.

Afif A, Hoffmann D, Minotti L, Benabid AL, Kahane P (2008) Middle short gyrus of the insula implicated in pain processing. Pain 138:546–555.

Afif A, Hoffmann D, Becq G, Guenot M, Magnin M, Mertens P (2009) MRI-based definition of a stereotactic two-dimensional template of the human insula. Stereotact Funct Neurosurg 87:385–394.

Allman JM, Watson KK, Tetreault NA, Hakeem AY (2005) Intuition and autism: a possible role for Von Economo neurons. Trends Cogn Sci 9:367–373.

Allman JM, Tetreault NA, Hakeem AY, Manaye KF, Semendeferi K, Erwin JM, Park S, Goubert V, Hof PR (2010) The von Economo neurons in frontoinsular and anterior cingulate cortex in great apes and humans. Brain Struct Funct 214:495–517.

Allman JM, Tetreault NA, Hakeem AY, Manaye KF, Semendeferi K, Erwin JM, Park S, Goubert V, Hof PR (2011) The von Economo neurons in the frontoinsular and anterior cingulate cortex. Ann N Y Acad Sci 1225:59–71.

Amunts K, Zilles K (2001) Advances in cytoarchitectonic mapping of the human cerebral cortex. Neuroimaging Clin N Am 11:151–169. vii.

Anderson K, Bones B, Robinson B, Hass C, Lee H, Ford K, Roberts TA, Jacobs B (2009) The morphology of supragranular pyramidal neurons in the human insular cortex: a quantitative Golgi study. Cereb Cortex 19:2131–2144.

Augustine JR (1985) The insular lobe in primates including humans. Neurol Res 7:2–10.

Blaizot X, Mansilla F, Insausti AM, Constans JM, Salinas-Alaman A, Pro-Sistiaga P, Mohedano-Moriano A, Insausti R (2010) The human parahippocampal region: I. Temporal pole cytoarchitectonic and MRI correlation. Cereb Cortex 20:2198–2212.

Bonthius DJ, Solodkin A, Van Hoesen GW (2005) Pathology of the insular cortex in Alzheimer disease depends on cortical architecture. J Neuropathol Exp Neurol 64:910–922.

Brooks JC, Zambreanu L, Godinez A, Craig AD, Tracey I (2005) Somatotopic organisation of the human insula to painful heat studied with high resolution functional imaging. NeuroImage 27:201–209.

Butti C, Hof PR (2010) The insular cortex: a comparative perspective. Brain Struct Funct 214:477–493.

Butti C, Santos M, Uppal N, Hof PR (2013) Von Economo neurons: Clinical and evolutionary perspectives. Cortex 49:312–326.

Cauda F, D'Agata F, Sacco K, Duca S, Geminiani G, Vercelli A (2011) Functional connectivity of the insula in the resting brain. NeuroImage 55:8–23.

Cerliani L, Thomas RM, Jbabdi S, Siero JC, Nanetti L, Crippa A, Gazzola V, D'Arceuil H, Keysers C (2012) Probabilistic tractography recovers a rostrocaudal trajectory of connectivity variability in the human insular cortex. Hum Brain Mapp 33:2005–2034.

Chiry O, Tardif E, Magistretti PJ, Clarke S (2003) Patterns of calcium-binding proteins support parallel and hierarchical organization of human auditory areas. Eur J Neurosci 17:397–410.

Cloutman LL, Binney RJ, Drakesmith M, Parker GJ, Lambon Ralph MA (2012) The variation of function across the human insula mirrors its patterns of structural connectivity: evidence from *in vivo* probabilistic tractography. Neuroimage 59:3514–3521.

Craig AD (2009) How do you feel-now? The anterior insula and human awareness. Nat Rev Neurosci 10:59–70.

Craig AD, Chen K, Bandy D, Reiman EM (2000) Thermosensory activation of insular cortex. Nat Neurosci 3:184–190.

Eickhoff S, Walters NB, Schleicher A, Kril J, Egan GF, Zilles K, Watson JD, Amunts K (2005) High-resolution MRI reflects myeloarchitecture and cytoarchitecture of human cerebral cortex. Hum Brain Mapp 24:206–215.

Eickhoff SB, Amunts K, Mohlberg H, Zilles K (2006a) The human parietal operculum. II. Stereotaxic maps and correlation with functional imaging results. Cereb Cortex 16:268–279.

Eickhoff SB, Schleicher A, Zilles K, Amunts K (2006b) The human parietal operculum. I. Cytoarchitectonic mapping of subdivisions. Cereb Cortex 16:254–267.

Evrard HC, Forro T, Logothetis NK (2012) Von Economo neurons in the anterior insula of the macaque monkey. Neuron 74:482–489.

Fatterpekar GM, Naidich TP, Delman BN, Aguinaldo JG, Gultekin SH, Sherwood CC, Hof PR, Drayer BP, Fayad ZA (2002) Cytoarchitecture of the human cerebral cortex: MR microscopy of excised specimens at 9.4 T. AJNR Am J Neuroradiol 23:1313–1321.

Friedman DP, Murray EA (1986) Thalamic connectivity of the second somatosensory area and neighboring somatosensory fields of the lateral sulcus of the macaque. J Comp Neurol 252:348–373.

Friedman DP, Murray EA, O'Neill JB, Mishkin M (1986) Cortical connections of the somatosensory fields of the lateral sulcus of macaques: evidence for a corticolimbic pathway for touch. J Comp Neurol 252:323–347.

Frot M, Mauguiere F (2003) Dual representation of pain in the operculo-insular cortex in humans. Brain 126:438–450.

Frot M, Magnin M, Mauguiere F, Garcia-Larrea L (2007) Human SII and posterior insula differently encode thermal laser stimuli. Cereb Cortex 17:610–620.

Fullerton BC, Pandya DN (2007) Architectonic analysis of the auditory-related areas of the superior temporal region in human brain. J Comp Neurol 504:470–498.

Galaburda A, Sanides F (1980) Cytoarchitectonic organization of the human auditory cortex. J Comp Neurol 190:597–610.

Gallay MN, Jeanmonod D, Liu J, Morel A (2008) Human pallidothalamic and cerebellothalamic tracts: anatomical basis for functional stereotactic neurosurgery. Brain Struct Funct 212:443–463.

Gallay DS, Gallay MN, Jeanmonod D, Rouiller EM, Morel A (2012) The insula of Reil revisited: multiarchitectonic organization in macaque monkeys. Cereb Cortex 22:175–190.

Garcia-Larrea L, Perchet C, Creac'h C, Convers P, Peyron R, Laurent B, Mauguiere F, Magnin M (2010) Operculo-insular pain (parasylvian pain): a distinct central pain syndrome. Brain 133:2528–2539.

Geyer S, Weiss M, Reimann K, Lohmann G, Turner R (2011) Microstructural parcellation of the human cerebral cortex – from Brodmann's post-mortem map to in vivo mapping with high-field magnetic resonance imaging. Front Hum Neurosci 5. http://dx.doi.org/10.3389/fnhum.2011.00019.

Glasser MF, Van Essen DC (2011) Mapping human cortical areas in vivo based on myelin content as revealed by T1- and T2-weighted MRI. J Neurosci 31:11597–11616.

Jakab A, Molnar PP, Bogner P, Beres M, Berenyi EL (2012) Connectivity-based parcellation reveals interhemispheric differences in the insula. Brain Topogr 25:264–271.

Kim EJ, Sidhu M, Gaus SE, Huang EJ, Hof PR, Miller BL, Dearmond SJ, Seeley WW (2012) Selective frontoinsular von economo neuron and fork cell loss in early behavioral variant frontotemporal dementia. Cereb Cortex 22:251–259.

Kurth F, Zilles K, Fox PT, Laird AR, Eickhoff SB (2010a) A link between the systems: functional differentiation and integration within the human insula revealed by meta-analysis. Brain Struct Funct 214:519–534.

Kurth F, Eickhoff SB, Schleicher A, Hoemke L, Zilles K, Amunts K (2010b) Cytoarchitecture and probabilistic maps of the human posterior insular cortex. Cereb Cortex 20:1448–1461.

Mackey S, Petrides M (2009) Architectonic mapping of the medial region of the human orbitofrontal cortex by density profiles. Neuroscience 159:1089–1107.

Mazzola L, Isnard J, Peyron R, Guenot M, Mauguiere F (2009) Somatotopic organization of pain responses to direct electrical stimulation of the human insular cortex. Pain 146:99–104.

Mazzola L, Isnard J, Peyron R, Mauguiere F (2012a) Stimulation of the human cortex and the experience of pain: Wilder Penfield's observations revisited. Brain 135:631–640.

Mazzola L, Faillenot I, Barral FG, Mauguiere F, Peyron R (2012b) Spatial segregation of somato-sensory and pain activations in the human operculo-insular cortex. Neuroimage 60:409–418.

Mesulam MM, Mufson EJ (1982a) Insula of the old world monkey. I. Architectonics in the insulo-orbito-temporal component of the paralimbic brain. J Comp Neurol 212:1–22.

Mesulam MM, Mufson EJ (1982b) Insula of the old world monkey. III: Efferent cortical output and comments on function. J Comp Neurol 212:38–52.

Mesulam MM Mufson EJ (1985) The insula of Reil in man and monkey. Architectonics, connectivity, and function. In: Cerebral cortex (Peters A, Jones E, eds), pp 179–224. Plenum Publishing Corporation.

Morel A (2007) Stereotacic Atlas of the Human Thalamus and Basal Ganglia. New York: Informa Healthcare USA, Inc..

Morosan P, Rademacher J, Schleicher A, Amunts K, Schormann T, Zilles K (2001) Human primary auditory cortex: cytoarchitectonic subdivisions and mapping into a spatial reference system. Neuroimage 13:684–701.

Morosan P, Schleicher A, Amunts K, Zilles K (2005) Multimodal architectonic mapping of human superior temporal gyrus. Anat Embryol (Berl) 210:401–406.

Mufson EJ, Mesulam MM (1982) Insula of the old world monkey. II: Afferent cortical input and comments on the claustrum. J Comp Neurol 212:23–37.

Mufson EJ, Mesulam MM (1984) Thalamic connections of the insula in the rhesus monkey and comments on the paralimbic connectivity of the medial pulvinar nucleus. J Comp Neurol 227:109–120.

Mutschler I, Wieckhorst B, Kowalevski S, Derix J, Wentlandt J, Schulze-Bonhage A, Ball T (2009) Functional organization of the human anterior insular cortex. Neurosci Lett 457:66–70.

Naidich TP, Kang E, Fatterpekar GM, Delman BN, Gultekin SH, Wolfe D, Ortiz O, Yousry I, Weismann M, Yousry TA (2004) The insula: anatomic study and MR imaging display at 1.5 T. AJNR Am J Neuroradiol 25:222–232.

Nguyen DK, Nguyen DB, Malak R, Leroux JM, Carmant L, Saint-Hilaire JM, Giard N, Cossette P, Bouthillier A (2009) Revisiting the role of the insula in refractory partial epilepsy. Epilepsia 50:510–520.

Nieuwenhuys R (2012a) The insular cortex: A review. In: Progress in Brain Research (Hofman MA, Falk D, eds), pp 123–163. Elsevier.

Nieuwenhuys R (2012b) The myeloarchitectonic studies on the human cerebral cortex of the Vogt-Vogt school, and their significance for the interpretation of functional neuroimaging data. Brain Struct Funct. http://dx.doi.org/10.1007/s00429-012-0460-z.

Nimchinsky EA, Vogt BA, Morrison JH, Hof PR (1995) Spindle neurons of the human anterior cingulate cortex. J Comp Neurol 355:27–37.

Ongur D, Ferry AT, Price JL (2003) Architectonic subdivision of the human orbital and medial prefrontal cortex. J Comp Neurol 460:425–449.

Ostrowsky K, Magnin M, Ryvlin P, Isnard J, Guenot M, Mauguiere F (2002) Representation of pain and somatic sensation in the human insula: a study of responses to direct electrical cortical stimulation. Cereb Cortex 12:376–385.

Peyron R, Laurent B, Garcia-Larrea L (2000) Functional imaging of brain responses to pain. A review and meta-analysis (2000). Neurophysiol Clin 30:263–288.

Pugnaghi M, Meletti S, Castana L, Francione S, Nobili L, Mai R, Tassi L (2011) Features of somatosensory manifestations induced by intracranial electrical stimulations of the human insula. Clin Neurophysiol 122:2049–2058.

Rivier F, Clarke S (1997) Cytochrome oxidase, acetylcholinesterase, and NADPH-diaphorase staining in human supratemporal and insular cortex: evidence for multiple auditory areas. Neuroimage 6:288–304.

Santos M, Uppal N, Butti C, Wicinski B, Schmeidler J, Giannakopoulos P, Heinsen H, Schmitz C, Hof PR (2011) Von Economo neurons in autism: a stereologic study of the frontoinsular cortex in children. Brain Res 1380:206–217.

Schleicher A, Palomero-Gallagher N, Morosan P, Eickhoff SB, Kowalski T, de Vos K, Amunts K, Zilles K (2005) Quantitative architectural analysis: a new approach to cortical mapping. Anat Embryol 210:373–386.

Schmued L, Bowyer J, Cozart M, Heard D, Binienda Z, Paule M (2008) Introducing Black-Gold II, a highly soluble gold phosphate complex with several unique advantages for the histochemical localization of myelin. Brain Res 1229:210–217.

Schulz G, Crooijmans HJ, Germann M, Scheffler K, Muller-Gerbl M, Muller B (2011) Three-dimensional strain fields in human brain resulting from formalin fixation. J Neurosci Methods 202:17–27.

Seeley WW (2010) Anterior insula degeneration in frontotemporal dementia. Brain Struct Funct 214:465–475.

Simms ML, Kemper TL, Timbie CM, Bauman ML, Blatt GJ (2009) The anterior cingulate cortex in autism: heterogeneity of qualitative and quantitative cytoarchitectonic features suggests possible subgroups. Acta Neuropathol 118:673–684.

Small DM (2010) Taste representation in the human insula. Brain Struct Funct 214:551–561.

Stephani C, Fernandez-Baca Vaca G, Maciunas R, Koubeissi M, Luders HO (2011) Functional neuroanatomy of the insular lobe. Brain Struct Funct 216:137–149.

Ture U, Yasargil DC, Al-Mefty O, Yasargil MG (1999) Topographic anatomy of the insular region. J Neurosurg 90:720–733.

Uylings HBM, Sanz-Arigita EJ, de Voos K, Pool CW, Evers P, Rajkowska G (2010) 3-D Cytoarchitectonic parcellation of human orbitofrontal cortex. Coorrelation with postmortem MRI. Psychiatry Res:Neuroimaging 183:1–20.

Veldhuijzen DS, Greenspan JD, Kim JH, Lenz FA (2010) Altered pain and thermal sensation in subjects with isolated parietal and insular cortical lesions. Eur J Pain 14(535):e531–511.

Von Economo C (2009) Cellular structure of the human cerebral cortex. Translated by L.C. Triarhou. In: Karger, Basel.

Von Economo C, Koshinas G (1925) Die Cytoarchitektonik der Hirnrinde des Erwachsenen Menschen. In: Springer, Berlin.

Wallace MN, Johnston PW, Palmer AR (2002) Histochemical identification of cortical areas in the auditory region of the human brain. Exp Brain Res 143:499–508.

Walters NB, Egan GF, Kril JJ, Kean M, Waley P, Jenkinson M, Watson JD (2003) In vivo identification of human cortical areas using high-resolution MRI: an approach to cerebral structure-function correlation. Proc Natl Acad Sci U S A 100:2981–2986.

Zaki J, Davis JI, Ochsner KN (2012) Overlapping activity in anterior insula during interoception and emotional experience. Neuroimage 62:493–499.